Preprint:
Wainman, L., Ilyinskaya, E., Pfeffer, M. et al. (2025) Heterogeneous trace element deposition from an effusive volcanic plume. [Preprint - Research Square]

https://doi.org/10.21203/rs.3.rs-6665526/v1

Heterogeneous trace element deposition from an effusive volcanic plume

Laura Wainman

eelrw@leeds.ac.uk

University of Leeds

Evgenia Ilyinskaya

University of Leeds https://orcid.org/0000-0002-3663-9506

Melissa Pfeffer

Icelandic Meteorological Office https://orcid.org/0000-0002-1689-1739

Celine Mandon

Icelandic Meteorological Office

Eniko Bali

Nordvulk, Institute of Earth Sciences, University of Iceland https://orcid.org/0000-0001-7289-6393

Penny Wieser

University of California, Berkeley https://orcid.org/0000-0002-1070-8323

Brock Edwards

Centre for Earth Observation Science, Department of Environment and Geography, University of Manitoba

Martin Voigt

Institute of Earth Sciences, University of Iceland

Barbara Kleine-Marshall

Friedrich-Alexander University

Sylvia Guðjónsdóttir

Institute of Earth Sciences, University of Iceland

Abigail Symons

School of Earth and Environment, University of Leeds

Adam Cotterill

Department of Earth Sciences, University College London

Samantha Hammond

Open University

Barbara Kunz

Open University https://orcid.org/0000-0002-9492-1497

Frances Jenner

The Open University https://orcid.org/0000-0003-2189-6478

Anja Schmidt
https://orcid.org/0000-0001-8759-2843
Andri Stefánsson
University of Iceland
Emma Nicholson
University College London https://orcid.org/0000-0003-1749-9285
Sæmundur Halldórsson
Nordic Volcanological Center, Institute of Earth Sciences, University of Iceland https://orcid.org/0000-0002-9311-7704
Jóhann Gunnarsson Robin
Nordic Volcanological Center, Institute of Earth Sciences, University of Iceland, Reykjavík, Iceland
https://orcid.org/0000-0003-0594-0950
Alessandro Aiuppa
Dipartimento DiSTeM, Università di Palermo https://orcid.org/0000-0002-0254-6539
Michael Burton
University of Manchester https://orcid.org/0000-0003-3779-4812
Tamsin Mather
University of Oxford https://orcid.org/0000-0003-4259-7303

Article

Keywords:

Posted Date: May 28th, 2025

DOI: https://doi.org/10.21203/rs.3.rs-6665526/v1

Additional Declarations: There is **NO** Competing Interest.

Heterogeneous trace element deposition from an effusive volcanic plume

Laura Wainman[a], Evgenia Ilyinskaya[a], Melissa Anne Pfeffer[b], Celine Mandon[b], Enikö Bali[c], Penny Wieser[d], Brock Edwards[e,f], Martin Voigt[c], Barbara Kleine-Marshall[g], Sylvía Guðjónsdóttir[c], Abigail Symons[a] Adam S. Cotterill[h], Samantha J. Hammond[i], Barbara Kunz[i], Frances Jenner[i], Anja Schmidt[j,k,l], Andri Stefánsson[c], Emma Nicholson[h,p], Sæmundur Halldórsson[c], Jóhann Gunnarsson Robin[c], Alessandro Aiuppa[m], Mike Burton[n], Tamsin A. Mather[o].

[a]School of Earth and Environment, University of Leeds, Leeds, UK.
[b]Icelandic Meteorological Office, Reykjavík, Iceland.
[c]Institute of Earth Sciences, University of Iceland, Reykjavik, Iceland.
[d]Earth and Planetary Science, UC Berkeley, Berkeley, USA.
[e]Centre for Earth Observation Science, Department of Environment and Geography, University of Manitoba, Winnipeg, Canada.
[f]Geological Survey of Canada, Natural Resources Canada, Ottawa, Canada.
[g]GeoZentrum Nordbayern, Friedrich-Alexander University Erlangen-Nuremberg, Erlangen, Germany
[h]Department of Earth Sciences, University College London, London, UK.
[i]School of Environment, Earth and Ecosystem Sciences, The Open University, Milton Keynes, UK.
[j]Yusuf Hamied Department of Chemistry, Cambridge, CB2 1EW, UK
[k]Institute of Atmospheric Physics (IPA), German Aerospace Centre (DLR), 82234 Oberpfaffenhofen, Germany
[l]Meteorological Institute, Ludwig Maximilian University of Munich, 80333 Munich, Germany
[m]Università degli Studi di Palermo, Dipartimento di Scienze della Terra e del Mare, Palermo, Italy.
[n]Department of Earth and Environmental Sciences, University of Manchester, Manchester, UK
[o]Department of Earth Sciences, University of Oxford, Oxford, UK.
[p]School of Graduate Research, University of Waikato, Hamilton, New Zealand

Corresponding author: Laura Wainman (eelrw@leeds.ac.uk)

Abstract

Effusive basaltic eruptions are an important source of volatile trace elements to the troposphere. Constraining the effects of background atmospheric conditions on the transport behavior and plume lifetimes of these elements is critical, both in the use of trace elements as proxies in the geological record, and in mitigating exposure to these elements in downwind communities. Through in-situ multi-element sampling of the Fagradalsfjall (Iceland) 2021-2022 eruption plumes we present the first direct comparison of element dispersion behavior under wet and dry atmospheric conditions. We demonstrate that the alkali metals (Na, K, Rb, Cs) are depleted up to an order of magnitude more under wet background conditions compared to elements such as Se, As, and Cd, which are instead lost preferentially in drier conditions. We propose that heterogeneous element deposition from the volcanic plume is driven by the interactions between element gas-phase speciation, water solubility of the resulting complexes, particulate size-distribution, and affinity for scavenging by larger ash particles. For volcanoes situated in regions with distinct seasonal weather patterns, the delivery of elements to the surface, and thus human exposure to potentially toxic metals such as arsenic, lead, cadmium, and selenium, could therefore vary between wet and dry conditions.

Main Text

Emissions of gas and particulate matter (PM) from effusive basaltic eruptions are an important natural source of volatile elements to the troposphere[1,2]. Elements may be released both as silicate material (e.g. ash) or in the gas phase, either as free gases, or more commonly, complexed as oxides, halides, sulfides, or hydroxides[3-6]. Upon emission, these magmatic gases cool through mixing with the atmosphere and may undergo rapid droplet condensation and gas-to-particle conversion[7]. The resulting aerosol PM is transported downwind in the volcanic plume and may be dispersed 10's to 100's km[2,8-11,78]. During transport, wet and dry depositional processes remove PM (as well as gas phase species) from the plume and thus deliver a range of elements to the surface[2,8,9,12,13]. The additional input of these elements may act as essential nutrients for land and ocean ecosystems[14] or can accumulate to harmful levels in biological and hydrological reservoirs[8-9,15-19, 38-41]. Over 10% of the world's population live within 100 km of an active volcano[20] and thus may be exposed to elevated levels of trace metals via volcanic emissions, contaminated water or soil[21]. Understanding the processes that facilitate element deposition to the environment is therefore critical to constraining their atmospheric lifetimes and dispersion patterns. This has implications both for mitigating human exposure during volcanic unrest and in the use of trace elements as proxies in the geological record[72-75].

The deposition of trace elements from the atmosphere may be facilitated by both wet and dry processes[12,15,22,23]. Dry deposition occurs via gravitational settling, where the largest particles generally have the shortest residence times in the atmosphere[22]. Wet deposition is facilitated via wash-out by hydrometeors such as rain and snow as they fall through the plume[8,13]. Recent investigation of the evolution of Kīlauea's plume during the 2018 eruption has challenged assumptions that trace elements are removed from the plume homogeneously during these processes. The observed fractionation in trace element composition of Kīlauea plume suggests that the higher volatility elements (e.g., Cd, Te, Se) which form the more soluble complexes, may be lost preferentially in high-humidity conditions due to plume wash-out[2]. Inherent element characteristics (such as size-resolved mass distribution, magmatic volatility, and water solubility) as well as external factors, such as localized topography and background atmospheric conditions, are likely to play a role in governing element dispersion patterns and relative rates of deposition[12,15]. The ground-based sampling campaign at Kīlauea was not able to directly track fractionation occurring within the volcanic plume, because the nearest downwind sample was collected 40 km from the vent at Kīlauea. Equally, it was not possible to compare trace element behavior under wet and dry atmospheric conditions during the same eruption[2]. Thus, uncertainty remains over the temporal and spatial scales over which heterogeneous deposition occurs, and the impact of differing meteorological conditions.

The varied meteorological conditions during the Fagradalsfjall 2021 – 2022 eruptions[46] provided an exceptional opportunity to directly compare trace element plume behavior under both wet and dry atmospheric conditions within the same volcanic system. Effusive plumes of gas (H_2O, SO_2, CO_2, H_2S, HCl, HF) and aerosol PM were produced during both

eruptions[79,80] and were dispersed in the lower troposphere, reaching Grindavik (12 km downwind) and the capital city, Reykjavik (45 km) on several occasions[24,25]. Our samples were collected within 2 km of the active vent(s) allowing us to constrain heterogenous deposition and plume fractionation within the near-vent effusive plume. UAV (uncrewed aerial vehicle) sampling allowed for unprecedented access to the volcanic plume which would have been impossible with only ground-based sampling techniques[26,27] (see Fig 1). Fresh snow fall, which interacted with the volcanic plume during deposition, was also collected in the early phases of the 2021 eruption, allowing for a direct comparison of element deposition under wet and dry conditions, respectively.

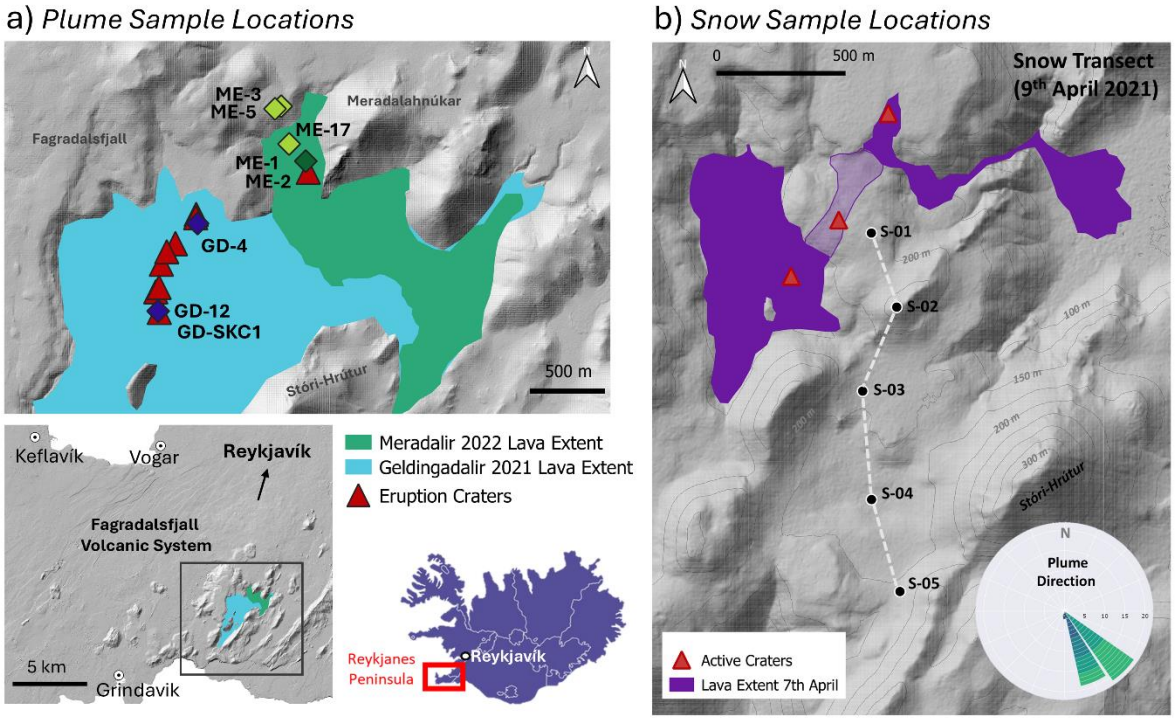

Figure 1. Plume and snow sampling locations. a) shows filter pack (FP) and cascade impactor (SKC) plume sampling locations for the 2021 and 2022 eruptions, with the lava extent and active crater locations for each eruption also shown. See Supplementary Table 1 for sample overviews. Broader geographic context of the eruptions within the Fagradalsfjall volcanic system on the Reykjanes peninsula is shown below, including proximities to nearby towns. b) shows snow sampling set up during the 2021 eruption using a transect beneath the plume. Wind rose diagram shows the plume direction rather than conventional meteorological wind, where the transect was collected parallel to the prevailing wind direction. Solid purple fill shows mapped lava extent on 7th April 2021, dashed fill shows additional approximate lava extent at the time of sampling on the 9th April 2021. Composite DEM from[43-45]. The collection of samples following fresh snowfall is vital to avoid contamination between different snow-plume interactions and has previously been used to investigate the composition of volcanic plumes[13] and the global dispersal of trace metals to ice cores[72-75].

Results

Magmatic Volatility, Water Solubility, and Particulate Size Distribution

An element's magmatic volatility may be described by its emanation coefficient (ε_x) which quantifies the proportion of the element that is released from the magma into the gas phase[28-30]. Figure 2a compares element emanation coefficients for the Fagradalsfjall 2021-2022 eruptions with those reported for other global volcanoes. Emanation coefficients were calculated using an average of two at-vent filter pack (FP) measurements for both 2021 and 2022 eruptions and represent the mass % of each element degassed from the erupting lava (See Methods M6 for details of emanation calculation and weighted ash fraction (WAF) correction using matrix glass compositions). The least volatile elements are those with coefficients < 0.001% and include major elements such as Fe, as well as rare earth elements (REE) Nd, Sm, La, and Ce. Most other elements fall within the moderately to highly volatile range with emanation coefficients between 0.001% and 10%. The lower end of this range is made up of the alkali metals Li, Na, Rb, and Cs, whilst the more volatile elements include metals and metalloids Zn, Sn, Pb, and As. The most volatile elements are those with emanation coefficients > 10% and include Cd, Se, and Te.

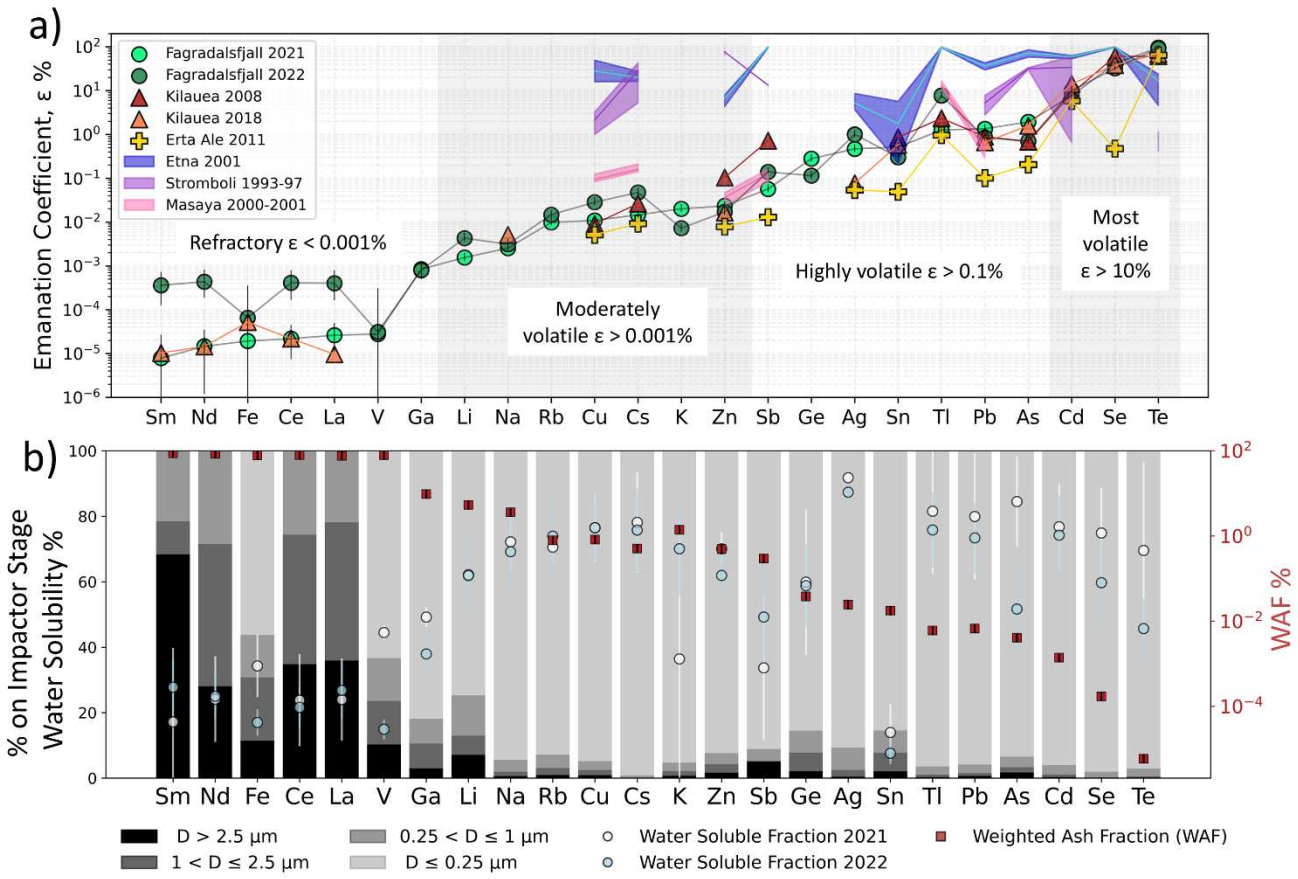

Figure 2. Element emanation coefficient, size distribution, water solubility, and ash fraction. a) Emanation coefficients calculated using average of two at-source FP samples for each Fagradalsfjall eruption (2021: GD-4, GD-12. 2022: ME-1, ME-2) with a weighted ash fraction (WAF) correction applied using matrix glasses from lava samples collected during the same eruption (see Methods, M6). Red triangles show coefficients calculated for the 2018 Kīlauea eruption[31] and 2008 eruption[9]. Yellow pluses for the Erta Ale 2011 eruption[32] and shaded lines show coefficients for arc volcanoes Etna 2001[33,34], Stromboli 1993-97[35], and Masaya 2000-2001[4]. b) Size distribution data from SKC impactor sample (GD-SKC1) where grey bars show the % mass of each element found within a given size bin. The concentration of refractory elements collected in the coarsest size fraction is likely to be under sampled by the SKC impactor due to increased wall deposition

in the coarsest impactor stage[42] (See Supplementary Fig. 1). Elements are ordered by increasing emanation coefficient. Red squares show WAF, the proportion of the element concentration on the filter pack that is attributed to the silicate ash and dust component of the plume, calculated as an average of two filter pack samples (GD-4 and GD-12). Water solubility is calculated as the percentage of that element found in the water-soluble component of the total extraction (where the total extraction is the water and acid soluble components combined) and is shown by white circles (2021 – average of GD-4 and GD-12) and blue circles (2022 – ME-1 and ME-2), with the error bars showing the range between the two filter pack samples (See Methods, M4).

Previous investigations have shown that the more volatile elements (ε_x > 1%), such as Se, Te, Cd, Pb, and As, are predominantly hosted in the smallest size fraction of the aerosol PM and have the highest water solubilities[2,9,36]. In contrast, the most refractory elements, including Fe, Ce, La, Nd, Sm (ε_x < 0.001%) are generally found in the coarsest ash-rich size fraction and are less water soluble[2,9,36]. Figure 2b shows the water solubility, mass % size distribution, and the weighted ash fraction (WAF; the proportion of the element on the filter attributed to silicate ash) for a subset of trace elements. The REE, which are some of the most refractory elements, show the highest concentrations in the coarsest size fraction, with all PM exceeding 0.25 μm and most being > 1 μm in diameter. Other refractory elements found predominantly in the coarsest fraction are V and Fe, although these do have a (~ 50%) sub-0.25 μm component. Across all refractory elements the weighted ash fraction is ~ 100%, indicative of being hosted predominantly in the silicate ash component of the plume[2,9]. A general decrease in the contribution of silicate ash is seen with increasing element volatility, reflecting a greater contribution from condensed magmatic gases to the overall element concentration[15]. For example, the most volatile elements (Se, Te, Cd, As) have WAF < 1%, consistent with being hosted predominantly in the smaller (mostly < 0.25 μm) non-silicate aerosol fraction formed through gas-to-particle conversion[37]. The most refractory elements also show consistently lower water solubilities (< 50%) than the more volatile elements (> 60%). However, within the volatile fraction, the elements that have the lowest WAF and highest magmatic volatilities (e.g. Te, Se, Cd), are not consistently the most soluble (for example, Ag, Cs, Cu, Tl, and Pb all have higher water solubilities than Te). Sn and Sb also deviate from the overall trend of increased volatility, higher water solubility, and lower WAF, showing much lower solubilities and larger size fractions compared to similarly volatile elements.

Near-vent trace element deposition

Figure 3a shows the UAV sampling set up in the downwind airborne plume. Figure 3b shows the percentage of each element lost due to deposition from the plume at 500 m downwind, where the symbol size denotes the average particle diameter (from at-vent SKC sample, Fig. 2b). Estimates of element deposition from the airborne plume within the first 500 m downwind during the 2022 eruption range between 0 and 17%, and thus suggest that ~ 83-99 % of volcanogenic trace elements may be subject to longer-range dispersion in the troposphere. Dilution of the plume due to mixing with air is calculated as 20 +/- 5% between the vent (ME-1) and 500 meters (ME-3) based on the multi-GAS SO_2 concentration measurements (Methods M2 and Supplementary Fig. 2). Assuming homogenous dilution of the plume as it mixes downwind, theoretical downwind element concentrations may therefore be calculated as 20 +/- 5 % of those measured at-vent. Measured element concentrations in the downwind airborne plume were subtracted

from these theoretical diluted concentrations, with the difference being the percentage of that element lost from the plume via deposition. Over the first 500 m in the downwind plume the most refractory elements, Ti, Fe, Mn, and REEs show the greatest percentage loss from the volcanic plume (13-17%) compared to the more volatile elements (e.g., Ag, As, Zn, Se) which range from 0-13% (Fig. 3b). Even within the volatile aerosol fraction, however, this varies between elements. For example, Sn, Se, and Te are the most depleted of the volatile fraction with 11-13% lost from the plume within 500 m, whilst other volatile elements Ag, Cu, and Cs show < 5 % loss under the same atmospheric conditions.

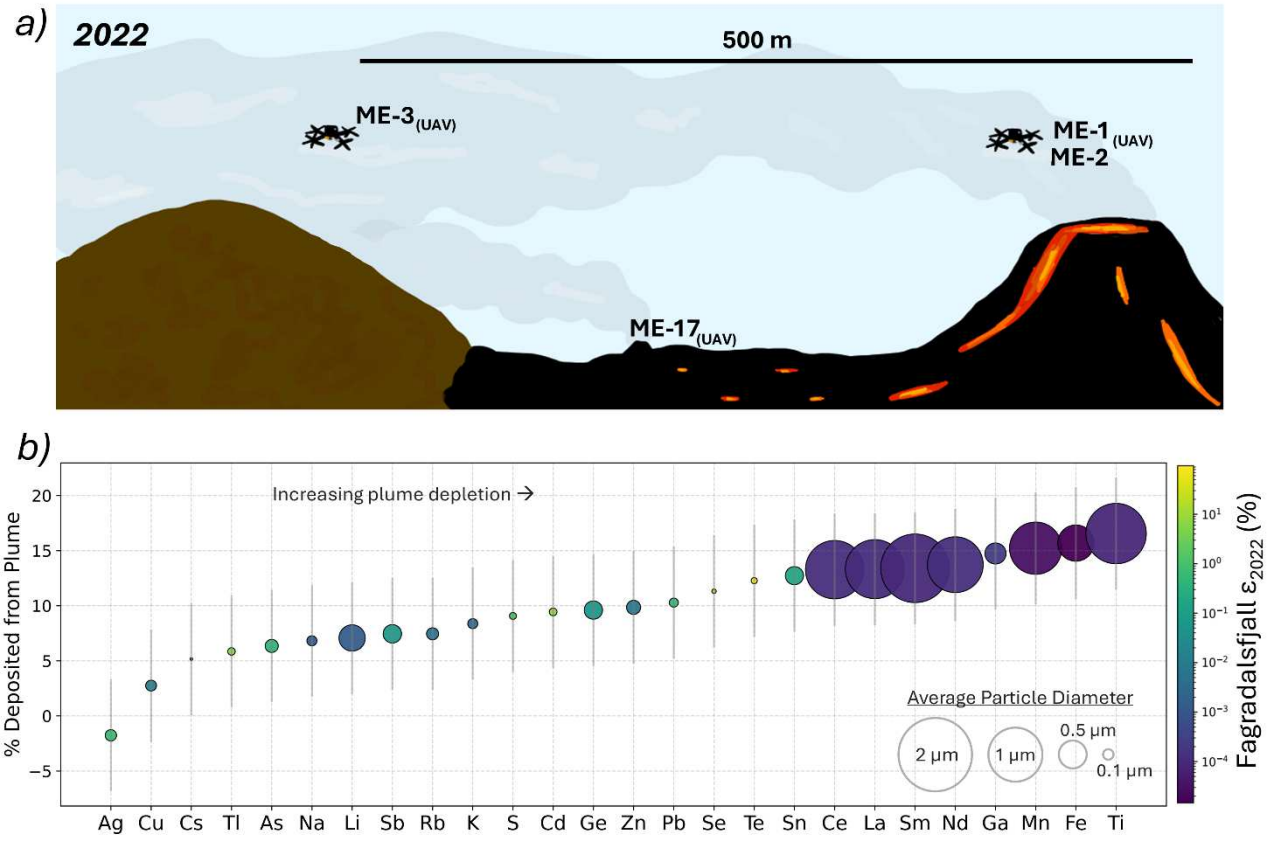

Figure 3. Element Deposition from the downwind airborne plume. a) Dry sampling set up during the 2022 eruption with FP samples being collected at-vent as well as in the downwind plume. b) Percentage deposited of each element from the airborne plume at 500 m downwind (increasing depletion from plume towards the right). Circle size denotes average particles size, as calculated using the distribution of elements across stages in SKC impactor sample GD-SKC1. Circles are colored according to the emanation coefficient ε_{2022} as calculated in Methods, M7 and shown in Fig. 2a. Error bars show % deposited from the plume assuming dilution to 20 +/- 5 % of original at-vent concentrations.

Wet deposition through snow-plume scavenging

During the 2021 eruption, ground-based snow samples were collected within 2 km of the vent along a transect following prevailing wind direction (Fig. 4a). Figure 4b shows element enrichments in the snow (at site S-02) relative to the basaltic lava on the y-axis and element enrichment in the plume relative to basalt on the x-axis, with both

enrichment factors normalized to Mg as the refractory reference element (see Methods, M7 for EF_{Mg} calculation). If elements are homogenously scavenged from the plume by the falling snow, they should lie on a straight line with a gradient of 1 (i.e. parallel to the 1:1 line), with an offset dictated by the degree of overall depletion in the snow vs the plume. For example, if the fallen snow contains 1% scavenged plume material with no relative fractionation between elements, symbols would plot on the 1:100 line. The refractory elements (Fe, Ti, Mn, REE) plot between the 10:1 and the 1:1 line, indicating that these elements are more enriched in the snow than expected from the scenario where the snow simply samples a diluted plume. In contrast, the more volatile elements cluster around the 1:100 line, indicating significantly greater depletion in the snow relative to the plume. It is notable that there is a clear skew from a 1:1 gradient with the most volatile elements such as Se, Cd, and Pb plotting below the 1:100 line, and the less volatile elements such as Zn, Cu, Rb, and Na plotting above the 1:100 line. This indicates that elements with lower emanation coefficients are more effectively scavenged by falling snow.

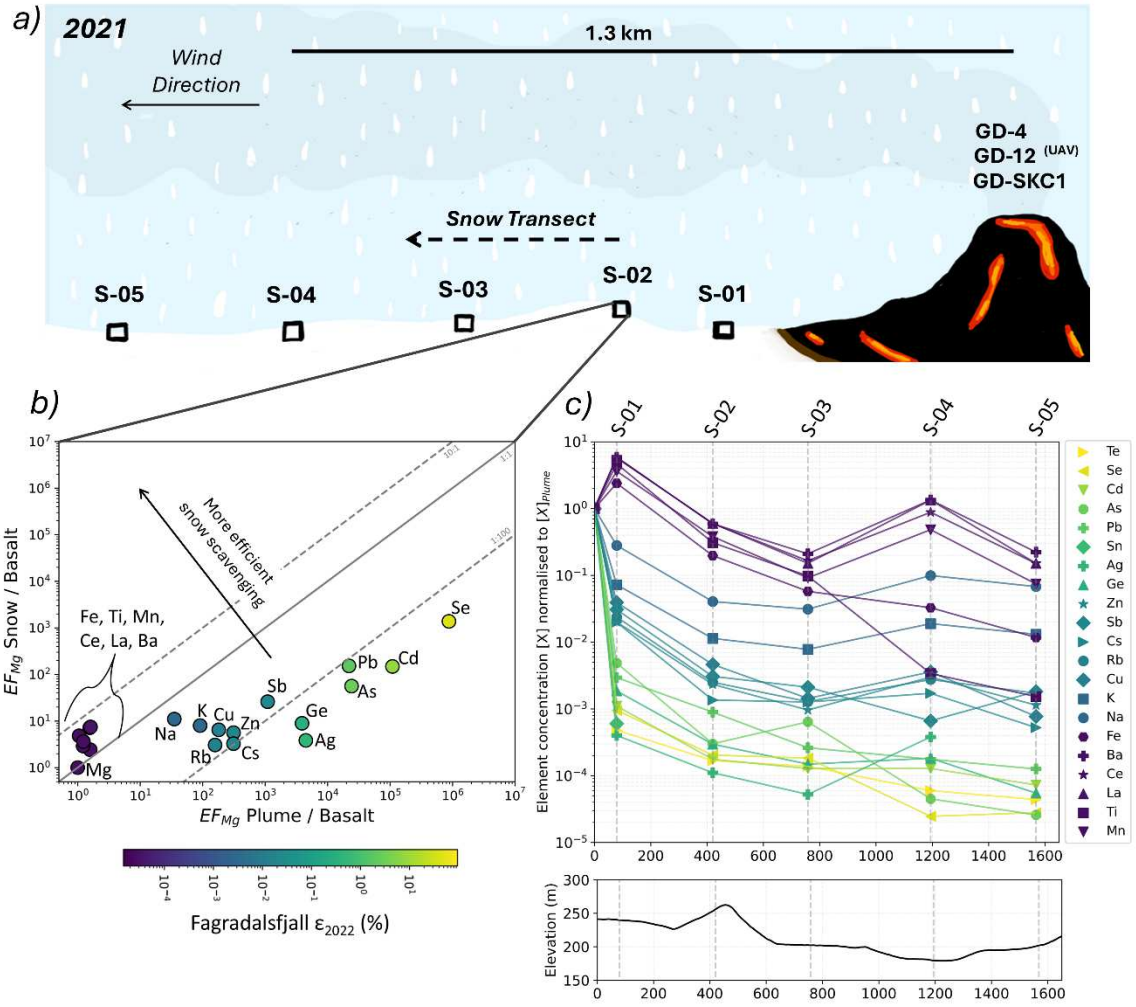

Figure 4. Element Deposition due to snow-plume interaction. a) sampling of wet deposition set up during the 2021 eruption, collecting a transect of snow samples from beneath the plume. At-vent FP and SKC samples were also collected using UAV platforms, although these were not collected during a snow fall event. b) Heterogeneous scavenging of elements from the plume by falling snow. Enrichment Factors, EF, were

calculated as outlined in Methods M7, relative to Mg as a refractory reference element. Y-axis shows EF for the snow sample S-02, and X-axis shows EF for the plume sample ME-1, relative to element concentrations in the basaltic lava. Elements are colored by their emanation coefficients calculated in Methods, M7 and shown in Fig. 2a. c) Concentrations of elements deposited via snow scavenging with increasing distance from the vent. Y-axis shows element concentration [X] in the snow sample normalized to element concentration in the at-vent plume sample. X-axis is distance from the vent. Elements are colored by emanation coefficient calculated in Methods, M7 and shown in Fig. 2a for the 2021 eruption. All snow samples were collected on the 9th April 2021 between 12 and 2 pm following fresh snowfall. Lower panel shows elevation change along the transect route shown in Fig. 1b for snow sample collection.

Figure 4c shows that element concentrations in ground-based snow samples, normalized to element concentrations in the at-vent plume sample, generally decrease with increasing distance from the vent, and that the rate of decrease varies significantly between elements. For example, at 800 m downwind, deposited concentrations of elements relative to the at-vent plume sample show: four orders of magnitude decrease for Se and Te; three orders of magnitude decrease for Cu, Cs, and Rb; and only one order of magnitude for decrease for the refractory elements Fe, Mn and REE. This disparity between elements continues downwind, but the rate of decrease for most elements out beyond 800 m downwind, with the exception of Ce, Mn, and La which show an increase in deposited concentrations at 1200 m downwind that is not observed for any of the more volatile elements.

Discussion

Gas Phase Speciation

Within the non-silicate aerosol PM fraction of the volcanic plume, heterogenous element deposition appears to be strongly dependent on background atmospheric conditions. Under dry atmospheric conditions airborne sampling showed thar elements such as Sn, Se, Te, and Pb are preferentially deposited from the plume (Fig 3b), whilst under wetter background conditions sampled the alkali metals (Na, K, Rb, Cs) are more efficiently removed via snow scavenging through the plume (Fig 4b). Thermochemical modelling of the gas-phase chemistry of the Fagradalsfjall volcanic plume[47] shows that Cs, Cu, and Rb have an affinity for complexing as chloride species (M-Cl), whilst Se, Te, Sn, and Pb show more variable speciation behavior, forming sulfide (M- S(-II)), sulfate (M-S(+VI)) and oxide (M-O) complexes[31,47] . The water solubility of elements hosted in the aerosol PM phase may therefore be tied to gas phase speciation behavior. For example, the alkali metals (Na, K, Rb, Cs), which predominantly complex with Cl in the gas phase, are known to form soluble salts upon decompression and cooling[51-53]. These are the most soluble of the elements measured in the Fagradalsfjall volcanic plume (Fig. 2b) and are also the most readily scavenged from the aerosol PM by falling snow (Fig 4b). In contrast, other elements, such as Se, Sn, Cd, As, and Pb, show more variable gas phase speciation behavior as sulfides, sulfates, oxides, and hydroxides, and form less soluble or insoluble salts[9,53]. However, thermodynamic data for gas-phase species—particularly sulfur compounds—are often lacking and commonly rely on extrapolations from lower temperatures[48-50]. In addition, speciation is typically modelled only in the gas phase (as in this study), potentially omitting important complexes and overlooking changes during gas-to-particle conversion. Expanding thermodynamic datasets and modeling these

transitions will be essential for more accurately constraining element speciation in aerosol PM.

Wet Vs Dry Deposition

Previous work has shown that Cl-bearing gases are scavenged to a greater extent during wet deposition than S-bearing gases because of their higher solubility in water[12,54,55,82]. The higher solubilities of elements that complex with Cl in the gas phase may therefore explain their increased removal from aerosol PM as snow falls through the plume, where snow scavenging can occur via Brownian diffusion, impaction, and interception[54,55,83]. In rainfall that had fallen through the plume of Mt Etna the alkali metals Na, K, Cs and Rb also showed a higher degree of enrichment in the rain relative to elements Pb, Se and Cd[8]. In rain and snow samples, from Mt Etna and Fagradalsfjall, respectively, the refractory elements are also relatively more enriched than would be expected if scavenging from the volcanic plume was the only process delivering them to the surface[8] (Fig.4b). Elevated concentrations of these elements may suggest an additional contribution of geogenic dust or sea spray aerosol. Given the proximity of the snow samples to the main volcanic vent, rapid silicate ash fallout from the overhead plume may also have delivered some of these refractory elements to the surface, where larger ash particles will be more effectively removed by falling snow via impact scavenging[54,55]. The increase in refractory element concentrations in the snow sample 1200 m downwind also occurs at a relative topographic low (to the east of Stóri-Hrútur on Fig.1b). Increased concentrations in this sample may therefore be the result of resuspension and deposition of ash from surrounding topographic highs[63]. The turbulence of local wind patterns as they interact with topography, means that the dynamics of resuspension and deposition remain a considerable challenge to element dispersion modelling.

Under dry atmospheric conditions PM deposition is driven by gravitational settling and particle size distribution[12,15,22]. For example, within 500 m of the vent, the refractory elements (Fe, Mn, REE) are the most significantly depleted from the volcanic plume, with over 13% deposited (Fig 3b). These elements are hosted in the larger silicate ash fraction of the plume and will therefore settle out more quickly under gravity. Using Stoke's Law (see Supplementary Table 2) and an ash particle of 100 μm diameter the vertical settling time over 30 m is ~ 1-2 mins whilst for a particle within the aerosol PM fraction, with a diameter of 0.1 μm, settling out over the same distance would take ~ 10 days. Over the first 500 m downwind, minimal deposition of elements hosted predominantly in the aerosol PM fraction is therefore expected and is consistent with observations of elements such as Cs, Cu, and Ag, which show ≤ 5% deposition and have average diameters < 0.1 μm. However, elements such as Se, Te and Sn show much greater rates of deposition (11-13% over the first 500 m) despite being highly volatile and hosted in the smallest size fraction (0.25 μm). The differences in deposition behaviour between these elements may again be determined by their gas-phase speciation: Cs, Cu, and Ag have a greater affinity for Cl, whilst Sn, Se, and Te complex as sulfates and sulphides. Previous work has shown that dry deposition may account for a greater proportion of total S deposition from volcanic plumes compared to Cl[56] because S species are more readily adsorbed onto ash compared to Cl[57-59]. Thus, it follows that trace elements that have an affinity for

complexing with S may also be removed via adsorption onto larger ash particles that settle out more quickly under gravity.

The observed heterogenous deposition of trace elements within only 500 m downwind of the volcanic plume also highlights the importance and complexities of collecting unmodified "at-vent" samples. Modern UAV sampling approaches allow for collection within < 50 m of the vent and thus minimise the potential effects of heterogenous element deposition [26,27]. Prior to the use of UAVs for volcanic plume sampling, campaigns relying on ground sampling approaches only likely collected "at-vent" > 100-200 m from the vent for safety and access reasons. This could have led to an under reporting of some elements, having already been preferentially lost from the plume due to heterogenous near-vent deposition, and thus require subsequent post-sampling correction (based on 13-17% greater deposition of refractory elements reported above) when comparing to more modern datasets.

Implications for Environmental Distribution and Exposure

Our results highlight that both daily and seasonal changes in background atmospheric conditions may modulate trace element deposition to the surface. Seasonal controls on precipitation have already been shown to be a key determinant of the bulk amount of trace elements deposited, where less rainfall leads to atmospheric accumulation and lower rates of deposition[60]. Many volcanoes are in regions where the annual climate varies between distinct wet and dry seasons, meaning that the downwind dispersion and delivery of metals to the surface may also vary between seasons. This is particularly important for continuously outgassing open-vent volcanoes[76], such as Etna (Italy)[8,18] or Masaya (Nicaragua)[4,61,62] where nearly 1 million people live within 10 km of the volcano[81] and thus within potential dispersion distance of the volcanic plume. Health studies in communities around Masaya volcano have shown that chronic exposure to volcanic pollution may lead severe health impacts, particularly in the most vulnerable populations[21,77]. It is notable for example, that whilst food samples tested for heavy metal had concentrations below world health organisation guidelines, sample collection was carried out during the dry season, when the delivery of many heavy metals is likely to be at its lowest[77]. The varied wet and dry deposition behavior of different elements also highlights that certain exposure pathways (e.g., water or airborne) may be relatively more enriched in certain elements. For example, increased wash out of alkali metals Na, K, Li, Cs, and Rb in the wet season could concentrate these pollutants in precipitation, which may then be used for household water or drinking supplies[8,19]. The importance of this exposure route may however be underestimated if sampling occurred in the dry season, or if airborne exposure was the primary focus. Accounting for heterogeneous deposition of potentially toxic metals under different atmospheric conditions and via different pathways is therefore critical to advancing monitoring and hazard mitigation efforts. In places with less defined seasons but highly variable daily weather conditions, such as in Iceland, this weather-driven impact on the fall out and deposition of toxic metals is relevant for day-to-day short-term hazard assessment.

Methods

M1. Filter Packs. Filter packs (FP) mounted on UAS (DJI Matrice 600 Pro in 2021, DJI Matrice 300 RTK in 2022 and 2023) were used to collect in-situ samples of gases and aerosol PM in the near-vent volcanic plumes at the 2021 and 2022 Fagradalsfjall eruptions. The UAS was used to hover within the volcanic plume (assessed visually during flying using the on-board camera) both directly above the main active vent and to up to 1 km away in the downwind plume. Sampling altitude ranged between 50 and 200 m above the flight take off point. Total sampling duration ranged from 14 to 62 minutes for UAV-mounted FP samples, although due to UAS battery life limitations, most samples were the cumulation of multiple flights to the same location (see Supplementary Table 1). The sampling set up consisted of a 4-stage Teflon filter pack holder secured to the UAV "leg", connected via plastic tubing to a SKC Leland Legacy pump mounted on the body of the UAV (See Supplementary Fig. 5). The combined weight of the filter pack and pump (and on-board Multi-GAS) was just lower than the payload capacities of the UAVs (2.7 kg). Thus, care had to be taken to ensure a balanced weight distribution on the UAV to avoid issues upon take-off and landing.

A ground-based FP sample was also collected during the 2022 eruption. This was done using a portable backpack frame with the same filter pack and pump set up as the UAV samples (See Supplementary Fig. 5). The backpack frame allowed a "drop and go approach" where the frame could be placed in the area of grounding plume, without requiring prolonged supervision and thus risking extended human exposure to the plume. The duration of this sample was 26 minutes, with a flow rate of 10 L/min, and is thus comparable in volume and duration to the UAV-mounted samples.

The 4-stage filter packs were used in two different configurations: either containing just one filter for PM collection (PM Filter specifications: Whatman™ WTP polytetrafluoroethylene (PTFE) 47-mm diameter, pore size 1.0 µm) or with an additional 3 filters loaded behind the first PM filter for gas collection (Gas Filter Specifications: Whatman™ Quantitative Filter Papers, Ashless, Grade 41, 55-mm diameter (2021) and 47-mm diameter (2022), Millipore 47-mm diameter absorbent pads (2023)). The filters for gas collection were impregnated (5% K_2CO_3 + 1% glycerol in 2021, 5% KOH + 1% glycerol in 2022 and 2023) shortly prior to use (as used in Ilyinskaya et al.,[2], Mason et al.,[31]). Base treatment of gas filters allows for the capture of acidic gases such as SO_2, HCl and HF by reaction and conversion to their anions SO_4^{2-}, SO_3^{2-}, Cl^-, and F^-. Gas filters were considered saturated if > 10% of total SO_4^{2-} was present on the final gas filter stage (as defined by Mason et al.,[31]). All gas filters collected in 2021 were saturated, and thus we decided to use KOH rather than K_2CO_3 impregnation for the gas filters in 2022. Gas filters in 2022 did not saturate despite being exposed to comparable SO_2 concentrations across similar flight durations. Airflow through the filter pack was generated using an SKC Leland Legacy pump, also mounted on the UAS (see Table 1 for individual sample flow rates). The flow rate was set to the highest value that the pump was able to sustain (6 – 13.5 L/min). The highest sustained flow rate varied according to which filter set up was used (i.e., 1 or 4 filters loaded) and was also sensitive to the curvature of the connective tubing between pump and filter when mounting the equipment on the drone. Immediately after sampling, filter packs were sealed using Parafilm to prevent particle loss and contamination during transport.

M2. Multi-GAS. A Multi-GAS instrument from University of Palermo (Aiuppa et al.,[65], Liu et al.,[26], the same unit type used in Burton et al.,[64]) was co-located on the drone for time-series measurements of major gas concentrations (time resolution 1 Hz). The Multi-GAS contains SO_2 and H_2S electrochemical sensors (T3ST/F-TD2G-1A and T3H-TC4E-1A; both City Technology, calibrated for 0 to 200 ppmv and 0 to 50 ppmv respectively, see Liu et al.,[26]), and an infrared spectrometer for CO_2 (Edinburgh Instruments, range 0–3000 ppmv).

Time-averaged in-plume SO_2 concentrations for each FP and SKC sample were calculated using the co-collected Multi-GAS SO_2 timeseries, excluding data < 0.5 ppmv (the baseline between in-plume peaks in SO_2) within the known flight-time window. Mason et al.,[40] and Edwards et al.,[66] use background thresholds of 1 ppmv and 1.3 ppmv, respectively. Using alternative baselines of 0 and 1 ppmv resulted in a difference of less than 1% in our corrected in-plume flight times. The time averaged SO_2 concentrations should be viewed as minimum values as some in-plume measurements were made when SO_2 concentrations were above the maximum detection limit of the sensor (saturation occurred at ~ 220 ppmv, % of time above Multi-GAS saturation recorded in Table 1). The total time FP and SKC samples spent inside the aerosol plume (defined as SO_2 > 0.5 ppmv) was used to correct the total volume pumped for the in-plume volume sampled.

M3. SKC Impactors. The use of cascade impactors is similar to that of filter packs, where the impactor is connected to an air pump which draws the volcanic plume through a series of stages containing PTFE filters. SKC impactors consist of 4 stages and an after stage and can thus resolve particles into a series of five size bins of decreasing particle diameter ranges - cut off diameters at 2.5 µm, 1.0 µm, 0.5 µm, and 0.25 µm (with all PM smaller than 0.25 µm collected on the final after-stage). Cascade impactors were used during the 2021 eruption campaign to collect a size resolved sample (S_M_SKC1) above the main volcanic vent for comparison with a similar FP sample (SFP12). Although the samples were collected on different days, they were collected within the same phase of the eruption and thus we would expect a similar at-vent composition. Comparison between the two samples is shown in Supplementary Fig. 1. The finest fraction containing the more volatile elements follows a 1:1 relationship in element concentration between FP and the SKC impactors, whereas the coarsest fraction, which predominantly consists of the more refractory elements is consistently under sampled (by up to 5 times) in the SKC impactor relative to their collection on the FP. This may be due to increased wall deposition in the coarsest stages of the impactor[42].

M4. Extraction and Compositional Analysis. The samples were handled in a class-10000 clean lab environment at the Institute of Earth Sciences, University of Iceland and the School of Earth and Environment, University of Leeds. Gas and PM filters were extracted following an established procedure[2,31]. All filters were cut into quarters and transferred to acid-cleaned 50 ml centrifuge tubes using acid-cleaned metal-free scissors and tweezers prior to the extraction process. Gas filters were leached in 20 ml Milli-Q (> 18.2 MΩ, MQ) water and 250 µl H_2O_2 (to oxidize collected sulfur species to sulfate) and then shaken for 20 mins. 1.5 ml from these solutions was pipetted for anion concentration measurements by ion chromatography (IC) at the Department of Geography, University of Leeds (on Thermo Dionex ICS5000) and Institute of Earth Sciences, University of Iceland (on Thermo Dionex ICS2000).

Material collected on PM filters was extracted using a two-stage sequential leaching method[2,31]. The water-soluble PM fraction was first extracted in 20 ml MQ water + 200 µl propan-2-ol (to reduce the hydrophobicity of the PM filters), shaken and placed in a sonic bath (20 mins each), before being centrifuged at 3000 rpm for 20 mins. 10 ml of the solution was then pipetted to 15 ml acid-clean tubes for analysis by ICP-QQQ MS (Agilent 8800), with another 1.5 ml pipetted for IC analysis (as described for the gas filters above). Water solubility of each element was calculated as the percentage of that element found in the water-soluble fraction, compared to the bulk PM extracted from the filter pack. The remaining solution and filters were transferred to an acid-cleaned 22 ml PFA vial. 5 ml UPA grade concentrated HNO_3 was added to the PFA beaker and samples dried on a hot plate at 55 °C. 1 ml UPA grade concentrated HNO_3 and 1 ml UPA grade concentrated HF were pipetted to the solid residue and refluxed for 3 h at 110 °C with lids on the PFA beakers. The lids were then removed, and samples dried at 55 °C. 10 ml UPA grade concentrated HNO_3 was then pipetted to the solid residue and refluxed on a hot plate at 90-100 °C

for sample back into solution. 10 ml MQ was pipetted into the PFA beakers and then transferred to an acid-cleaned sample tube for analysis by ICP-MS/MS.

PM filter samples and blanks were analyzed for major and trace elements by ICP-QQQ MS in the School of Environment, Earth and Ecosystem Sciences at the Open University, UK. Field, lab, and filter blanks were used to quantify the level of contamination at all stages of the sampling and extraction process and were found to be negligible. Synthetic calibration standards were doped with the same solution matrix as samples in order to eliminate ionization effects (particularly with samples containing propan-2-ol). Ionization effects were monitored by running an on-line internal standard throughout all measurement sessions. Elements were analyzed using a triple quad set up with different collision gas modes (no gas, O_2, and NH_3) to minimize polyatomic and isobaric interferences (add ref). This allows for lower detection limits and improved accuracy across the range of elements analyzed.

M5. Snow Sampling. During the 2021 eruption fresh snow samples were collected surrounding the active vent (within 2 km). The snow samples were collected in acid-washed (1M HCl, followed by rinsing in MQ water) plastic bags. Samples were collected along a transect at increasing distance from the main vent and parallel to wind direction on the 9th April 2021 between 12 pm and 2 pm local time. Collection following fresh snowfall through the plume is important for minimizing contamination and overlap between different plume events. Previous studies have employed a similar approach, using samples of snow which had freshly fallen through the plume to investigate the gaseous and trace element composition of the volcanic plume (Hekla, 2000 eruption[13]).

Samples bags were stored frozen until processing (< 1 week). Snow samples were unfrozen in warm water baths and immediately filtered through 0.45 um cellulose acetate filters. pH was measured at room temperature with a standard combination pH electrode, calibrated with buffer solutions at pH 4 and 7. Samples were analyzed for major and trace elements by ICP-MS/MS in the School of Environment, Earth and Ecosystem Sciences at the Open University, UK. Suprapur and DI blanks were used to quantify the level of contamination during the analysis process and were found to be negligible. Elements were analyzed using a triple quad set up with different collision gas modes (no gas, O_2, and NH_3) to minimize polyatomic and isobaric interferences. This allows for lower detection limits and improved accuracy across the range of elements analyzed.

M6. Weighted Ash Fraction (WAF) Correction. Matrix glass samples from both the 2021 and 2022 eruptions were analyzed for major and trace elements via JEOL JXA-8230 SuperProbe electron probe micro-analyzer (EPMA) at the Institute of Earth Sciences, University of Iceland[67] and LA-ICP-MS/MS (Agilent 8800) at the Open University using analytical techniques outlined in Jenner and O'Neill[68] for trace elements. The Ag analysis was done using a line scan on matrix glasses with the same approach as described in Wieser et al.[69] for Se analysis in melt inclusions. The ZrO interference correction was done as described in Reekie et al.[70], with reference material analyses for Ag from Jenner et al.[71]. These analyses were undertaken to determine an ash composition for each eruption (see sheets S6 and S7, supplementary information). Presumed ash compositions were used to perform subsequent weighted ash fraction corrections on all filter pack samples.

To constrain the concentration of elements in the non-silicate aerosol phase (i.e not contained in ash or dust) a weighted ash fraction (WAF) correction was applied to filter pack samples in this study. We assume via mass balance that for volatile elements the concentration on the filter, $[A]_{filter}$ in ppm is derived from two components, silicate ash and dust $[A]_{ash}$, and non-silicate aerosol $[A]_{aerosol}$ (see eq. 1).

$$[A]_{filter} = [A]_{ash} * X_{ash} + [A]_{aerosol} * (1 - X_{ash}) \qquad \text{eq. 1}$$

Where X_{ash} is mass fraction from silicate ash on the filter and $X_{aerosol}$, the mass fraction from the aerosol phase on the filter.

For refractory elements we assume that the concentration in aerosol phase is zero ($[A]_{aerosol} = 0$), allowing equation 1 to be simplified to:

$$X_{ash} = \frac{[A]_{filter}}{[A]_{ash}} \qquad \text{eq. 2 – only for refractory reference elements Fe, Mg, Mn, Ti}$$

Using the average of four refractory reference elements (Fe, Mg, Mn, Ti) it is then possible to derive Xash for each filter pack sample. Using an average of four major elements as our reference elements is beneficial as their higher concentrations (relative for example to REE) in silicate material allow smaller ash concentrations to be resolved. Weighted ash fractions for each element in each sample (WAF) can then be calculated using eq. 3 and inputting the X_{ash} calculated for each sample using the refractory reference elements:

$$WAF = 100 * \frac{X_{ash} * [A]_{ash}}{[A]_{filter}} \qquad \text{eq. 3}$$

Note that this means that whilst the overall mass fraction of ash on the filter may be low (< 1%) the WAF (contribution from ash for a specific element on the filter) may still be high, particularly for refractory elements (generally > 90%).

M7. Emanation Coefficients and Enrichment Factor Calculations. Emanation coefficients (ε_x) describe the degree to which an element is degassed from silicate melts into a vapour phase:

$$\varepsilon_X = \frac{([X]_i - [X]_f)}{[X]_i} \qquad \text{eq.4}$$

where $[X]_i$ is the initial concentration of X in the melt, and $[X]_f$ is the final degassed concentration of element X in the melt[29,30]. In this work, emanation coefficients (ε_x) are calculated using the measured composition of the volcanic plume (gas and PM), combined with the composition of degassed matrix glasses:

$$\varepsilon_X = \frac{[X/Y]_{plume} * Y_{degassed}}{[X]/[Y]_{plume} * Y_{degassed} + X_{MG}} \qquad \text{eq.5}$$

where X is the element of interest, and Y is S. X_{plume} is the concentration of element X measured on particulate filters (corrected for ash, as above); Y_{plume} is the total S measured on filter pack particulate and gas filters; and $Y_{degassed}$ is the concentration of S degassed during subaerial eruption (determined by comparison of melt inclusion and matrix glass compositions). X_{MG} is the concentration of element X remaining in the degassed matrix glass (See Supplementary Sheet S6). This approach assumes that the concentration of elements in the melt, and their degassing, scales linearly with S or Cl, which is likely to be a reasonable approximation in most cases.

Note also that emanation coefficients are calculated using silicate-corrected plume composition data, and therefore these emanation coefficients are relative, i.e., during the ash-correction, elements used to calculate X_{ash} are assumed to be only present in a silicate phase, and therefore these elements have emanation coefficients of zero (or close to zero) but may partition into the

gas phase to a limited extent. Emanation coefficients for the Fagradalsfjall 2021 and 2022 eruptions are included in Supplementary Sheet S4.

Enrichment factors (EF) describe the degree to which an element X is enriched in one phase relative to another, as calculated below. In this work we calculate EF both for the volcanic plume and snow compositions relative to the basaltic glass composition, using Mg as a refractory reference element:

$$EF_{Mg} = \frac{[X]_{Plume/Snow}/[X]_{Basalt}}{[Mg]_{Plume/Snow}/[Mg]_{Basalt}} \quad \text{eq.6}$$

Where $X_{plume/snow}$ are the concentrations of the element X in measured plume and snow samples and and X_{basalt} is the concentration in basaltic glass sampled from the same eruption.

Acknowledgements

Laura Wainman acknowledges that this work was supported by the Leeds–York–Hull Natural Environment Research Council (NERC) Doctoral Training Partnership (DTP) Panorama (grant no. NE/S007458/1) and the Icelandic Meteorological Office CASE Partnership. Evgenia Ilyinskaya also acknowledges support from Centre for Observation and Modelling of Earthquakes, Volcanoes and Tectonics (COMET) and NERC Urgency Grant NE/Z000262/1 "Chemistry of emissions at lava-urban interfaces". Analysis costs were also partially covered by the Icelandic Research Fund (RANNÍS): Magma dynamics on the Reykjanes Peninsula (MaDre) - Integrated geochemical and geophysical investigation of the (on-going) 2021 Fagradalsfjall eruption (grant nr: 228933-053). Adam Cotterill acknowledges support from the London NERC DTP and Brock Edwards from the Geological Survey of Canada (Environmental Geosciences Program), Natural Sciences and Engineering Research Council of Canada. Penny Wieser acknowledges support from a Sloan Research Fellowship. Alessandro Aiuppa acknowledges funding from the RETURN Extended Partnership funded by the European Union Next-GenerationEU (National Recovery and Resilience Plan – NRRP, Mission. We also thank Claire Horwell for kindly lending equipment to support our field campaigns, and the pilots at Svarmi. We thank the Icelandic Meteorological Office and the University of Iceland for their field campaign support and for providing the composite DEM used in Fig. 1b.

Author contributions

E.I led the 2021 field campaign and E.I and L.W jointly led the field campaign in 2022 with significant contributions from C.M, B.E, M.V, B.K.M, S.G, A.D, A.S across the two field campaigns. E.B and A.S contributed additional whole rock samples for their own field work. A.A, M.B, and T.A.M provided additional equipment during the field campaigns. P.W, S.H, B.K, F.J, S.H and J.G aided in carrying out the laboratory analysis which was led by L.W and supervised by E.I and C.M. Results analysis was led by L.W and supervised by E.I and M.A.P with contribution from A.S. Paper writing was led by L.W All authors participated in the discussion of the results and contributed to the paper.

Competing interests

The authors declare no competing interests.

Data availability

The authors declare that all data supporting the findings of this study are available within the paper and in Supplementary Data Sheet. Observational data of gas, PM, and snow composition are in the process of being deposited in the Centre for Environmental Data Analysis (CEDA) archive:

References

1. Nriagu, J.O. A global assessment of natural sources of atmospheric trace metals. *Nature*, 338(6210), pp.47–49. doi:https://doi.org/10.1038/338047a0 (1989).
2. Ilyinskaya, E., et al. Rapid metal pollutant deposition from the volcanic plume of Kīlauea, Hawai'i. Communications Earth & Environment, [online] 2(1), pp.1–15. doi:https://doi.org/10.1038/s43247-021-00146-2 (2021).
3. Mandon, C.L., Christenson, B.W., Schipper, C.I., Seward, T.M. and Garaebiti, E. Metal transport in volcanic plumes: A case study at White Island and Yasur volcanoes. *Journal of Volcanology and Geothermal Research*, 369, pp.155–171. doi:https://doi.org/10.1016/j.jvolgeores.2018.11.024 (2019).
4. Moune, S., Gauthier, P.-J. and Delmelle, P. Trace elements in the particulate phase of the plume of Masaya Volcano, Nicaragua. *Journal of Volcanology and Geothermal Research*, 193(3-4), pp.232–244. doi:https://doi.org/10.1016/j.jvolgeores.2010.04.004 (2010).
5. Symonds, R.B., Reed, M.H. and Rose, W.I., 1992. Origin, speciation, and fluxes of trace-element gases at Augustine volcano, Alaska: Insights into magma degassing and fumarolic processes. *Geochimica et Cosmochimica Acta*, *56*(2), pp.633-657.
6. Zelenski, M., Simakin, A., Taran, Y., Kamenetsky, V.S. and Malik, N.J.G.E.C.A., 2021. Partitioning of elements between high-temperature, low-density aqueous fluid and silicate melt as derived from volcanic gas geochemistry. *Geochimica et Cosmochimica Acta*, *295*, pp.112-134.
7. Symonds, R.B., Rose, W.I., Reed, M.H., Lichte, F.E. and Finnegan, D.L., 1987. Volatilization, transport and sublimation of metallic and non-metallic elements in high temperature gases at Merapi Volcano, Indonesia. *Geochimica et Cosmochimica Acta*, *51*(8), pp.2083-2101.
8. Calabrese, S., et al. Atmospheric sources and sinks of volcanogenic elements in a basaltic volcano (Etna, Italy). *Geochimica et Cosmochimica Acta*, 75(23), pp.7401–7425. doi:https://doi.org/10.1016/j.gca.2011.09.040 (2011).
9. Mather, T.A., et al. Halogens and trace metal emissions from the ongoing 2008 summit eruption of Kīlauea volcano, Hawai`i. *Geochimica et Cosmochimica Acta*, 83, pp.292–323. doi:https://doi.org/10.1016/j.gca.2011.11.029 (2012).
10. Hong, S., Candelone, J.-P. and Boutron, C.F. (1996). Deposition of atmospheric heavy metals to the Greenland ice sheet from the 1783–1784 volcanic eruption of Laki, Iceland. *Earth and Planetary Science Letters*, 144(3-4), pp.605–610. doi:https://doi.org/10.1016/s0012-821x(96)00171-9.
11. Ilyinskaya, E., et al. Understanding the environmental impacts of large fissure eruptions: Aerosol and gas emissions from the 2014–2015 Holuhraun eruption (Iceland). *Earth and Planetary Science Letters*, [online] 472, pp.309–322. doi:https://doi.org/10.1016/j.epsl.2017.05.025 (2017).
12. Delmelle, P. Environmental impacts of tropospheric volcanic gas plumes. *Geological Society, London, Special Publications*, 213(1), pp.381–399. doi:https://doi.org/10.1144/gsl.sp.2003.213.01.23 (2003).
13. Moune, S., Gauthier, Pierre-J., Gislason, S.R. and Sigmarsson, O. Trace element degassing and enrichment in the eruptive plume of the 2000 eruption of Hekla volcano, Iceland. *Geochimica et Cosmochimica Acta*, 70(2), pp.461–479. doi:https://doi.org/10.1016/j.gca.2005.09.011 (2006).
14. González-Santana, D., González-Dávila, M., González, A.G., Medina-Escuela, A., Fariña, D. and Santana-Casiano, J.M., 2024. Hot spot volcano emissions as a source of natural iron fertilization in the ocean. *Science of the Total Environment*, *957*, p.177638.
15. Mather, T.A., Pyle, D.M. and Oppenheimer, C. Tropospheric volcanic aerosol. In: *Volcanism and the Earth's Atmosphere*. [online] American Geophysical Union, pp.189–212. doi:https://doi.org/10.1029/139gm12 (2003).
16. Jones, M.T. and Gislason, S.R. Rapid releases of metal salts and nutrients following the deposition of volcanic ash into aqueous environments. Geochimica et Cosmochimica Acta, 72(15), pp.3661–3680. doi:https://doi.org/10.1016/j.gca.2008.05.030 (2008).

17. Martin, R.S., et al. Major and trace element distributions around active volcanic vents determined by analyses of grasses: implications for element cycling and bio-monitoring. *Bulletin of Volcanology*, 72(8), pp.1009–1020. doi:https://doi.org/10.1007/s00445-010-0374-7 (2010).
18. Calabrese, S., et al. Characterization of the Etna volcanic emissions through an active biomonitoring technique (moss-bags): Part 1 – Major and trace element composition. *Chemosphere*, 119, pp.1447–1455. doi:https://doi.org/10.1016/j.chemosphere.2014.08.086 (2015).
19. Liotta, M., et al. Mobility of plume-derived volcanogenic elements in meteoric water at Nyiragongo volcano (Congo) inferred from the chemical composition of single rainfall events. *Geochimica et Cosmochimica Acta*, 217, pp.254–272. doi:https://doi.org/10.1016/j.gca.2017.08.001 (2017).
20. Loughlin, S.C., Sparks, S., Brown, S., Jenkins, S. and Vye-Brown, C. *Global volcanic hazards and risk*. Cambridge: Cambridge University Press (2015).
21. Stewart, C., et al Volcanic air pollution and human health: recent advances and future directions. *Bulletin of Volcanology*, 84(1). doi:https://doi.org/10.1007/s00445-021-01513-9 (2021).
22. Wesely, M. and Hicks, B. A review of the current status of knowledge on dry deposition. *Atmospheric Environment*, 34(12-14), pp.2261–2282. doi:https://doi.org/10.1016/s1352-2310(99)00467-7 (2000).
23. Li, D., Zheng, J., Yang, M., Meng, Y., Yu, X., Zhou, H., Tong, L., Wang, K., Li, Y.-F., Wang, X. and Xiao, H. Atmospheric wet deposition of trace metal elements: Monitoring and modelling. The Science of The Total Environment, 893, pp.164880–164880.
24. Whitty, R et al., (in review) Fine-scale fluctuations of PM1, PM2.5, PM10 and SO2 concentrations caused by a prolonged volcanic eruption (Fagradalsfjall 2021, Iceland). EGUSphere.
25. Ilyinskaya, E., Snæbjarnarson, V., Carlsen, H. K., & Oddsson, B. Brief communication: Small-scale geohazards cause significant and highly variable impacts on emotions. Natural Hazards and Earth System Sciences Discussions, 2023, 1-12 (2023).
26. Liu, E.J., et al. Aerial strategies advance volcanic gas measurements at inaccessible, strongly degassing volcanoes. *Science Advances*, 6(44), p.eabb9103. doi:https://doi.org/10.1126/sciadv.abb9103 (2020).
27. Wainman, L. Using drones to sample volcanic plumes. *Nature Reviews Earth & Environment*, [online] 5(7), pp.484–484. doi:https://doi.org/10.1038/s43017-024-00570-w. (2024).
28. Edmonds, M., Mather, T.A. and Liu, E.J. A distinct metal fingerprint in arc volcanic emissions. *Nature Geoscience*, 11(10), pp.790–794. doi:https://doi.org/10.1038/s41561-018-0214-5 (2018).
29. Lambert, G., Le Cloarec, M.F., Ardouin, B. and Le Roulley, J.C. Volcanic emission of radionuclides and magma dynamics. *Earth and Planetary Science Letters*, 76(1-2), pp.185–192. doi:https://doi.org/10.1016/0012-821x(85)90158-x (1985).
30. Pennisi, M., Le Cloarec, M.F., Lambert, G. and Le Roulley, J.C. Fractionation of metals in volcanic emissions. *Earth and Planetary Science Letters*, 88(3-4), pp.284–288. doi:https://doi.org/10.1016/0012-821x(88)90085-4 (1988).
31. Mason, E., et al. Volatile metal emissions from volcanic degassing and lava–seawater interactions at Kīlauea Volcano, Hawai'i. *Communications Earth & Environment*, [online] 2(1), pp.1–16. doi:https://doi.org/10.1038/s43247-021-00145-3 (2021).
32. Zelenski, M.E., Fischer, T.P., de Moor, J.M., Marty, B., Zimmermann, L., Ayalew, D., Nekrasov, A.N. and Karandashev, V.K. Trace elements in the gas emissions from the Erta Ale volcano, Afar, Ethiopia. *Chemical Geology*, 357, pp.95–116. doi:https://doi.org/10.1016/j.chemgeo.2013.08.022 (2013).
33. Aiuppa, A. Gaetano, D. Valenza, M. Federico, C. and Pecoraino, G. Degassing of trace volatile metals during the 2001 eruption of Etna. *Volcanism and the Earth's Atmosphere*, 139, pp.41–54. doi:https://doi.org/10.1029/139gm03 (2003).
34. Aiuppa, A., Federico, C., Paonita, A., Pecoraino, G. & Valenza, M. S, Cl and F degassing as an indicator of volcanic dynamics: the 2001 eruption of Mount Etna. *Geophys. Res. Lett.* **29**, 54-1–54-4 (2002).
35. Allard, P., et al. Acid gas and metal emission rates during long-lived basalt degassing at Stromboli Volcano. *Geophysical Research Letters*, 27(8), pp.1207–1210. doi:https://doi.org/10.1029/1999gl008413 (2000).

36. Martin, R.S., et al. Composition-resolved size distributions of volcanic aerosols in the Mt. Etna plumes. Journal of Geophysical Research: Atmospheres, 113(D17) (2008).
37. Whitby, K.T. (1978). The physical characteristics of sulfur aerosols. *Atmospheric Environment (1967)*, 12(1-3), pp.135–159. doi:https://doi.org/10.1016/0004-6981(78)90196-8.
38. World Health Organisation. *Health risks of heavy metals from long-range transboundary air pollution.* [online] Available at: https://www.who.int/publications/i/item/9789289071796 (2007).
39. Department for Environment Food and Rural Affairs (DEFRA) (n.d.). *Heavy Metals Network*. [online] Available at: https://uk-air.defra.gov.uk/networks/network-info?view=metals.
40. US EPA (2015). *Metals*. [online] www.epa.gov. Available at: https://www.epa.gov/caddis/metals.
41. Vigneri, R., Malandrino, P., Gianì, F., Russo, M. and Vigneri, P. Heavy metals in the volcanic environment and thyroid cancer. *Molecular and Cellular Endocrinology*, [online] 457, pp.73–80. doi:https://doi.org/10.1016/j.mce.2016.10.027 (2017).
42. Berlinger, B., Torunn Kringlen Ervik, Kandler, K., Ulvestad, B., Benker, N., Ellingsen, D.G. and Bugge, M. Challenge with a Personal Cascade Impactor Sampler in a Silicon Metal Smelter. *Aerosol and Air Quality Research*, 21(6), pp.200577–200577. doi:https://doi.org/10.4209/aaqr.200577 (2021).
43. Náttúrufræðistofnun ÍslandsDEM version 1.0. https://gatt.lmi.is/geonetwork/srv/eng/catalog.search#/metadata/e6712430-a63c-4ae5-9158-c89d16da6361 Copied and adapted according to license CC-BY 4.0 (2020).
44. Sydney R. Gunnarson, Joaquín M. C. Belart, Birgir V. Óskarsson, Magnús Tumi Gudmundsson, Thórdís Högnadóttir, Gro B. M. Pedersen, Tobias Dürig, & Virginie Pinel. Automated processing of aerial imagery for geohazards monitoring: Results from Fagradalsfjall eruption, SW Iceland, August 2022 (1.1) [Data set]. Zenodo. https://doi.org/10.5281/zenodo.7871187 . (2023).
45. Pedersen, G. B. M., Belart, J. M. C., Óskarsson, B. V., Gudmundsson, M. T., Gies, N., Högnadóttir, T., et al. Volume, effusion rate, and lava transport during the 2021 Fagradalsfjall eruption: Results from near real-time photogrammetric monitoring. Geophysical Research Letters, 49, e2021GL097125. https://doi.org/10.1029/2021GL097125 (2022).
46. Halldórsson, S.A., Marshall, E.W., Caracciolo, A., Matthews, S., Bali, E., Rasmussen, M.B., Ranta, E., Robin, J.G., Guðfinnsson, G.H., Sigmarsson, O., Maclennan, J., Jackson, M.G., Whitehouse, M.J., Jeon, H., van der Meer, Q.H.A., Mibei, G.K., Kalliokoski, M.H., Repczynska, M.M., Rúnarsdóttir, R.H. and Sigurðsson, G. (2022). Rapid shifting of a deep magmatic source at Fagradalsfjall volcano, Iceland. Nature, [online] 609(7927), pp.529–534. doi:https://doi.org/10.1038/s41586-022-04981-x.
47. Wainman, L., et al. Trace Element Emissions Vary With Lava Flow Age and Thermal Evolution During the Fagradalsfjall 2021–2023 Eruptions, Iceland. *Geochemistry Geophysics Geosystems*, 25(12). doi:https://doi.org/10.1029/2024gc011822 (2024).
48. Symonds, R. B., & Reed, M. H. (1993). Calculation of multicomponent chemical equilibria in gas-solid-liquid systems; calculation methods, thermochemical data, and applications to studies of high-temperature volcanic gases with examples from Mount St. Helens. *American Journal of Science*, **293**(8), 758–864. **https://doi.org/10.2475/ajs.293.8.758**
49. Gerlach, T. M. (2004). Volcanic sources of tropospheric ozone-depleting trace gases. *Geochemistry, Geophysics, Geosystems*, **5**(9). **https://doi.org/10.1029/2004gc000747**
50. Martin, R. S., Mather, T. A., & Pyle, D. M. (2006). High-temperature mixtures of magmatic and atmospheric gases. *Geochemistry, Geophysics, Geosystems*, **7**(4), Q04006. **https://doi.org/10.1029/2005gc001186**
51. Higashi, H., Iwai, Y., Matsumoto, K., Kitani, Y., Okazaki, F., Shimoyama, Y. and Arai, Y., 2005. Measurement and correlation for solubilities of alkali metal chlorides in water vapor at high temperature and pressure. *Fluid phase equilibria*, *228*, pp.547-551.
52. Shimoyama, Y., Higashi, H., Tsuzaki, S., Okazaki, F., Kitani, Y., Iwai, Y. and Arai, Y., 2009. Effect of cation species on solubilities of metal chlorides in water vapor at high temperatures and pressures. *The Journal of Supercritical Fluids*, *50*(1), pp.1-5.
53. Desboeufs, K.V., Sofikitis, A., Losno, R., Colin, J.L. and Ausset, P. Dissolution and solubility of trace metals from natural and anthropogenic aerosol particulate matter. *Chemosphere*, 58(2), pp.195–203. doi:https://doi.org/10.1016/j.chemosphere.2004.02.025 (2005).

54. Cheng, I., Mamun, A.A. and Zhang, L. (2021). A synthesis review on atmospheric wet deposition of particulate elements: scavenging ratios, solubility, and flux measurements. Environmental Reviews, 29(3), pp.340–353. doi:https://doi.org/10.1139/er-2020-0118.
55. Zhang, L., Wang, X., Moran, M. D., & Feng, J. (2013). Review and uncertainty assessment of size-resolved scavenging coefficient formulations for below-cloud snow scavenging of atmospheric aerosols. Atmospheric Chemistry and Physics, 13(19), 10005-10025.
56. Kawaratani, R.K. and Fujita, S. Wet deposition of volcanic gases and ash in the vicinity of Mount Sakurajima. *Atmospheric Environment. Part A. General Topics*, 24(6), pp.1487–1492. doi:https://doi.org/10.1016/0960-1686(90)90057-t (1990).
57. Rose, W.I. Scavenging of volcanic aerosol by ash: Atmospheric and volcanologic implications. *Geology*, 5(10), p.621. doi:https://doi.org/10.1130/0091-7613(1977)5%3C621:sovaba%3E2.0.co;2 (1977).
58. Delmelle, P., Villieras, F. and Pelletier, M. Surface area, porosity and water adsorption properties of fine volcanic ash particles. *Bulletin of Volcanology*, 67(2), pp.160–169. doi:https://doi.org/10.1007/s00445-004-0370-x (2004).
59. Witham, C.S., Oppenheimer, C. and Horwell, C.J. Volcanic ash-leachates: a review and recommendations for sampling methods. *Journal of Volcanology and Geothermal Research*, 141(3-4), pp.299–326. doi:https://doi.org/10.1016/j.jvolgeores.2004.11.010 (2005).
60. Li, D., Zheng, J., Yang, M., Meng, Y., Yu, X., Zhou, H., Tong, L., Wang, K., Li, Y.-F., Wang, X. and Xiao, H. Atmospheric wet deposition of trace metal elements: Monitoring and modelling. The Science of The Total Environment, 893, pp.164880–164880. doi:https://doi.org/10.1016/j.scitotenv.2023.164880 (2023).
61. Martin, R.M., Sawyer, G.M., Spampinato, L., Salerno, G., Ramirez, C., Evgenia Ilyinskaya, Witt, M., Mather, T.A., Watson, I.J., Phillips, J.L. and Oppenheimer, C. A total volatile inventory for Masaya Volcano, Nicaragua. *Journal of Geophysical Research*, 115(B9) doi:https://doi.org/10.1029/2010jb007480 (2010a).
62. Martin, R.S., Mather, T.A., Pyle, D.M., Power, M., Tsanev, V.I., Oppenheimer, C., Allen, A.G., Horwell, C.J. and Ward, E.P.W. Size distributions of fine silicate and other particles in Masaya's volcanic plume. *Journal of Geophysical Research*, 114(D9). doi:https://doi.org/10.1029/2008jd011211 (2009).
63. Delmelle, P., Stix, J., Baxter, P., Garcia-Alvarez, J., & Barquero, J. Atmospheric dispersion, environmental effects and potential health hazard associated with the low-altitude gas plume of Masaya volcano, Nicaragua. Bulletin of Volcanology, 64, 423-434 (2002)
64. Burton, M., Allard, P., MuréF. and La Spina, A. Magmatic Gas Composition Reveals the Source Depth of Slug-Driven Strombolian Explosive Activity. *Science*, 317(5835), pp.227–230. doi:https://doi.org/10.1126/science.1141900 (2007).
65. Aiuppa, A. (2005). Chemical mapping of a fumarolic field: La Fossa Crater, Vulcano Island (Aeolian Islands, Italy). *Geophysical Research Letters*, 32(13). doi:https://doi.org/10.1029/2005gl023207.
66. Edwards, B.A., et al. Exceptionally low mercury concentrations and fluxes from the 2021 and 2022 eruptions of Fagradalsfjall volcano, Iceland. *Science of the total environment*, 917, pp.170457–170457. doi:https://doi.org/10.1016/j.scitotenv.2024.170457 (2024).
67. Halldórsson, S.A., Marshall, E.W., Caracciolo, A., Matthews, S., Bali, E., Rasmussen, M.B., Ranta, E., Robin, J.G., Guðfinnsson, G.H., Sigmarsson, O., Maclennan, J., Jackson, M.G., Whitehouse, M.J., Jeon, H., van der Meer, Q.H.A., Mibei, G.K., Kalliokoski, M.H., Repczynska, M.M., Rúnarsdóttir, R.H. and Sigurðsson, G. (2022). Rapid shifting of a deep magmatic source at Fagradalsfjall volcano, Iceland. Nature, [online] 609(7927), pp.529–534. doi:https://doi.org/10.1038/s41586-022-04981-x.
68. Jenner, F.E. and O'Neill, H.St.C. Analysis of 60 elements in 616 ocean floor basaltic glasses. *Geochemistry, Geophysics, Geosystems*, [online] 13(2), p.n/a-n/a. doi:https://doi.org/10.1029/2011gc004009 (2012).
69. Wieser, P.E., Jenner, F., Edmonds, M., Maclennan, J. and Kunz, B.E. Chalcophile elements track the fate of sulfur at Kīlauea Volcano, Hawai'i. *Geochimica et Cosmochimica Acta*, 282, pp.245–275. doi:https://doi.org/10.1016/j.gca.2020.05.018 (2020).

70. Reekie, C.D.J., Jenner, F.E., Smythe, D.J., Hauri, E.H., Bullock, E.S. and Williams, H.M. Sulfide resorption during crustal ascent and degassing of oceanic plateau basalts. *Nature Communications*, 10(1). doi:https://doi.org/10.1038/s41467-018-08001-3 (2019).
71. Jenner, F.E., Hauri, E.H., Bullock, E.S., König, S., Arculus, R.J., Mavrogenes, J.A., Mikkelson, N. and Goddard, C. The competing effects of sulfide saturation versus degassing on the behavior of the chalcophile elements during the differentiation of hydrous melts. *Geochemistry, Geophysics, Geosystems*, 16(5), pp.1490–1507. doi:https://doi.org/10.1002/2014gc005670 (2015).
72. Mason, E., Edmonds, M. and McConnell, J.R. (2022). Volatile trace metals deposited in ice as soluble volcanic aerosols during the 17.7.ka eruptions of Mt Takahe, West Antarctic Rift. Frontiers in Earth Science, 10. doi:https://doi.org/10.3389/feart.2022.1002366.
73. Vallelonga, P., Jean-Pierre Candelone, Van, Mark, Morgan, V. and Rosman, K.J.R. (2003). Lead, Ba and Bi in Antarctic Law Dome ice corresponding to the 1815 AD Tambora eruption: an assessment of emission sources using Pb isotopes. Earth and Planetary Science Letters, 211(3-4), pp.329–341. doi:https://doi.org/10.1016/s0012-821x(03)00208-5.
74. Rakociński, M., Pisarzowska, A., Corradini, C., Narkiewicz, K., Dubicka, Z. and Abdiyev, N. (2021). Mercury spikes as evidence of extended arc-volcanism around the Devonian–Carboniferous boundary in the South Tian Shan (southern Uzbekistan). Scientific Reports, 11(1). doi:https://doi.org/10.1038/s41598-021-85043-6.
75. Kellerhals, T., Tobler, L., Brütsch, S., Sigl, M., Wacker, L., Gäggeler, H.W. and Schwikowski, M. (2010). Thallium as a Tracer for Preindustrial Volcanic Eruptions in an Ice Core Record from Illimani, Bolivia. Environmental Science & Technology, 44(3), pp.888–893. doi:https://doi.org/10.1021/es902492n.
76. Edmonds, M., Liu, E.J. and Cashman, K.V. (2022). Open-vent volcanoes fuelled by depth-integrated magma degassing. Bulletin of Volcanology, 84(3). doi:https://doi.org/10.1007/s00445-021-01522-8.
77. van Manen, S.M. (2014). Perception of a chronic volcanic hazard: persistent degassing at Masaya volcano, Nicaragua. Journal of Applied Volcanology, 3(1). doi:https://doi.org/10.1186/s13617-014-0009-3.
78. Wu, K., Luo, Y., Li, Q., Zhou, H., Xi, L. and Si, F. (2025). Arctic haze induced by an Icelandic volcanic eruption: Evidence from China's highest-resolution trace gas monitoring. The Innovation Geoscience, pp.100131–100131. doi:https://doi.org/10.59717/j.xinn-geo.2024.100131.
79. Caracciolo, A., Bali, E., Ranta, E., S.A. Halldórsson, G.H. Guðfinnsson and B.V. Óskarsson (2024). Medieval and recent SO2 budgets in the Reykjanes Peninsula: implication for future hazard. Geochemical perspectives letters, 30, pp.20–27. doi:https://doi.org/10.7185/geochemlet.2417.
80. Pfeffer, M.A., Arellano, S., Barsotti, S., Guðrún Nína Petersen, Talfan Barnie, Evgenia Ilyinskaya, Tryggvi Hjörvar, Bali, E., Gro B.M. Pedersen, Guðmundsson, G.B., Kristín Vogfjörð, Eemu Johannes Ranta, Bergrún Arna Óladóttir, Edwards, B., Yves Moussallam, Andri Stefánsson, Samuel Warren Scott, Jean-Francois Smekens, Varnam, M. and Titos, M. (2024). SO2 emission rates and incorporation into the air pollution dispersion forecast during the 2021 eruption of Fagradalsfjall, Iceland. Journal of volcanology and geothermal research, 449, pp.108064–108064. doi:https://doi.org/10.1016/j.jvolgeores.2024.108064.
81. Global Volcanism Program, 2024. [Database] Volcanoes of the World (v. 5.2.8; 6 May 2025). Distributed by Smithsonian Institution, compiled by Venzke, E. https://doi.org/10.5479/si.GVP.VOTW5-2024.5.2
82. Textor, C., Graf, H.F., Herzog, M. and Oberhuber, J.M., 2003. Injection of gases into the stratosphere by explosive volcanic eruptions. *Journal of Geophysical Research: Atmospheres*, *108*(D19).
83. Paramonov, M., Grönholm, T. and Virkkula, A., 2011. Below-cloud scavenging of aerosol particles by snow at an urban site in Finland. Boreal Environ. Res, 16(4), pp.304-320.

Supplementary Files

This is a list of supplementary files associated with this preprint. Click to download.

- SupplementaryFile.xlsx
- SupplementaryDocument.docx